^{128}Xe and ^{130}Xe: Testing He-shell burning in AGB stars

R. REIFARTH

Los Alamos National Laboratory, Los Alamos, New Mexico, 87545, USA

reifarth@lanl.gov

F. KÄPPELER, F. VOSS, K. WISSHAK

Forschungszentrum Karlsruhe, Institut für Kernphysik, Postfach 3640, D-76021 Karlsruhe, Germany

R. GALLINO, M. PIGNATARI

Dipartimento di Fisica Generale, Università di Torino, Sezione INFN di Torino, Via P. Giuria 1, I-10125 Torino, Italy and Centre for Stellar and Planetary Astrophysics, School of Mathematical Sciences, Monash University 3800, Victoria, Australia

O. STRANIERO

Osservatorio Astronomico di Collurania, I-64100 Teramo, Italy

ABSTRACT

The *s*-process branching at ^{128}I has been investigated on the basis of new, precise experimental (n,γ) cross sections for the *s*-only isotopes ^{128}Xe and ^{130}Xe. This branching is unique, since it is essentially determined by the temperature- and density-sensitive stellar decay rates of ^{128}I and only marginally affected by the specific stellar neutron flux. For this reason it represents an important test for He-shell burning in AGB stars. The description of the branching by means of the complex stellar scenario reveals a significant sensitivity to the time scales for convection during He shell flashes, thus providing constraints for this phenomenon. The *s*-process ratio ^{128}Xe/^{130}Xe deduced from stellar models allows for a 9±3% *p*-process contribution to solar ^{128}Xe, in agreement with the Xe-S component found in meteoritic presolar SiC grains.

Subject headings: nucleosynthesis, *s* process, abundances, AGB stars: interiors, convection

1. Introduction

The long chain of the stable Xe isotopes exhibits the signatures of all scenarios contributing to the production of heavy elements beyond Fe, and is, therefore, of highest astrophysical interest. The light isotopes, ^{124}Xe and ^{126}Xe can be assigned to the p process, since they can not be produced via neutron capture. Their relative isotopic abundances are important for testing nucleosynthesis models describing the proton-rich side of the stability valley. Concerning the s process, xenon belongs to the six elements with a pair of s-only isotopes. In this case, the relevant nuclei are ^{128}Xe and ^{130}Xe, both shielded against the r-process region by their stable Te isobars. The abundances of these isotopes define the strength of the branching in the s-process reaction chain illustrated in Fig.1. Since the p-process contribution to the observed abundances in this mass region can typically be neglected, such shielded nuclei are commonly considered to be of pure s origin. In the case of Xe, however, it was pointed out that ^{128}Xe is not a typical s-only nucleus, since its solar abundance may include a significant p contribution (Woosley & Howard 1978). On the neutron-rich side, ^{134}Xe and ^{136}Xe are considered as r-only nuclei, since the β^- half life of ^{133}Xe is short enough to prevent any significant s-process production.

This paper aims at a thorough discussion of the s-process aspects by using accurate stellar (n,γ) cross sections of the relevant Te and Xe isotopes (Reifarth & Käppeler 2002; Reifarth et al. 2002). Following a summary of the various sources of isotopic Xe abundance patterns (§2), the particular features of the s-process branchings at $A = 127/128$ are discussed in §3. The s-process aspects related to thermally pulsing asymptotic giant branch (AGB) stars are described in §4, and the results are presented in §5.

2. Facts and observations

When stellar (n,γ) cross sections for ^{128,130}Xe with relative uncertainties of less then 2% became available (Reifarth et al. 2002), the determination of the elemental solar xenon abundance was a first natural application. While it is impossible to use standard methods for noble gases, i.e. meteorite analyses or solar spectroscopy, the solar Xe abundance of 5.30 $\pm$ 0.14 relative to Si=10^6 could be derived from s-process systematics. Apart from the solar abundance, these cross sections provide the key for the interpretation of the xenon isotope patterns, which bear promising clues for the analysis of presolar grains.

The noble gas nature of xenon implies that there are no stable chemical compounds. Accordingly, the isotopic ratios of xenon in planetary bodies were subject to mass fractionation effects during the earliest stages of the solar system. Terrestrial ratios are additionally

affected by fission of U and Th, which are both enriched compared to the solar average (De Laeter & Barnest 1991; Anders & Grevesse 1989). So far the most representative ratio for the solar system, $^{128}Xe/^{130}Xe = 0.510\pm0.005$, has been obtained from the solar wind component implanted in lunar rocks (Pepin et al. 1995; U. Ott, private communication). In the near future, more data are to be expected from the GENESIS mission (Rapp et al. 1996).

The discovery that presolar grains are carriers of noble gases with isotopic compositions significantly different from solar material (Ott 1993; Zinner 1998, and references therein) opened a new window to stellar and galactic evolution. These grains, which originate from circumstellar envelopes of AGB stars or supernova outflows by condensation of the most stable compounds, such as silicon carbide (SiC) and diamond (C), acted as carriers of trace elements like noble gases. Accordingly, their isotopic composition contains a wealth of information on the nucleosynthesis at the site of their origin. Among the many identified elements in these grains, the isotope patterns of the noble gases are particularly prominent. Two characteristic components were isolated for xenon (see Fig. 2 and Table 1):

- Xenon-S (Reynolds & Turner 1964) was found to be carried by presolar mainstream SiC grains (Lewis et al. 1994 and references therein), exhibits a pronounced zig-zag abundance pattern, reflecting the inverse of the respective stellar (n, γ) cross sections. This is characteristic for an s-process origin and points to AGB stars as the production site.

- Xenon-HL, which was identified in presolar diamond grains (Huss & Lewis 1994 and references therein). It exhibits enhanced abundances of the light and heavy isotopes and is most likely produced in supernova explosions, which are commonly believed to produce r- and p-enriched material.

Nucleosynthesis models are challenged by these observations, because the information contained in this material witnesses the original on-site production. As far as the s-process component is concerned, the challenge is directly linked to the reliability of the stellar neutron capture cross sections. The case of xenon is appealing, since the abundance ratio of the s-only nuclei ^{128}Xe and ^{130}Xe reflects the strength of the ^{127}Te and ^{128}I branchings as sketched in Fig. 1.

The presently available information on the $^{128}Xe/^{130}Xe$ ratio for Xe-S (Table 1) can not be explained by the schematic classical approach of the s process, which unavoidably overestimates this ratio at the characteristic temperature derived from the analysis of other branchings. More specific stellar evolutionary models have been invoked, using the Xe abundance patterns as a crucial model test.

3. The s-process branchings at ^{127}Te and ^{128}I

As illustrated in Fig. 1, the branchings at ^{127}Te and ^{128}I are expected to be comparably weak since only a small part of the total s-process flow is bypassing ^{128}Xe. Therefore, the product of the stellar (n,γ) cross section and the respective s abundance, which characterizes the reaction flow, is slightly smaller for ^{128}Xe than for ^{130}Xe. Since their solar isotopic abundance ratio (Pepin et al. 1995) as well as the stellar cross section ratio are accurately known, the $\langle\sigma\rangle N_s$ ratio, and hence the strength of the branching, can be determined.

The branching at ^{127}Te is weak, because the population of ground state and isomer is quickly thermalized in the hot stellar photon bath, leading to a strong dominance of the β-decay channel of the fast ground state decay. The neutron capture cross section of ^{127}Te is only theoretically known and may be uncertain by a factor of two. This branching plays an almost negligible role for the final ^{128}Xe/^{130}Xe ratio as we shall discuss later.

The second branching at ^{128}I with an half-life of only 25 min is exceptional, since it originates from the competition between the short-lived β^- and electron capture (EC) decays only. In contrast to other branchings, the influence of the stellar neutron flux is negligible in this case, thus eliminating an important uncertainty in the s-process calculation of the isotopic Xe abundances. This provides a unique possibility to better constrain temperature and electron density of the stellar plasma, which are manifested via the EC rate of ^{128}I (Takahashi & Yokoi 1987).

The branching factor at ^{128}I is

$$f_- = \frac{\lambda_{\beta^-}}{\lambda_{\beta^-} + \lambda_{\beta^{EC}}} = 1 - \frac{\lambda_{\beta^{EC}}}{\lambda_{\beta^-} + \lambda_{\beta^{EC}}}.$$

The β^--decay rate varies only weakly with stellar temperature, but the electron capture rate depends strongly on temperature due to the increasing degree of ionisation. Furthermore, at high temperatures, when the ions are fully stripped, the EC rate becomes sensitive to the density in the stellar plasma due to electron capture from the continuum. According to Takahashi & Yokoi (1987), the EC rate decreases by one order of magnitude at $T = 3 \times 10^8$ K and $\varrho = 3000$ gcm^{-3} with respect to the terrestrial value. Applying the simple expression for the branching strength, it appears that the branchings are working only at low temperatures (Table 2), at least in the straightforward constant-temperature concept of the classical model. Since a thermal energy of $kT = 29$ keV has instead been estimated by that approach (Arlandini et al. 1999; Best et al. 2001), it is obvious that the classical model fails in describing the ^{128}I branching. Indeed, using the new ^{128}Xe and ^{130}Xe cross sections, a fixed temperature of $kT = 29$ keV and a fixed matter density of 1.3×10^3 g/cm^3, one obtains an abundance ratio of $(^{128}\mathrm{Xe}/^{128}\mathrm{Xe})_s = 0.51\pm0.02$, as reported in Table 5.

This ratio matches the solar ratio, but not the Xe-S ratio of 0.447±0.003 measured in mainstream presolar grains. This problem can not be solved, even if one assumes a factor of two for uncertainty of the EC rate of ^{128}I, because this does not change the branching factor by more than 3%. It is worthwhile mentioning that in a recent investigation of the uncertainties of the decay rates calculated by (Takahashi & Yokoi 1987), the uncertainties of the stellar beta-decay rates of ^{128}I were estimated to be only ±10% (Goriely 1999).

Consequently, it needs to be checked, how this problem can be treated by the more comprehensive stellar *s*-process models.

4. The *s* process in thermally pulsing AGB stars

4.1. Models used

Current stellar models for describing the main *s*-process component in the mass range $A \geq 90$ refer to helium shell burning in thermally pulsing low mass AGB stars (Iben & Renzini 1983; Busso et al. 1999). This scenario is characterized by the subsequent operation of two neutron sources during a series of helium shell flashes. First, the ^{13}C(α, n)^{16}O reaction occurs under radiative conditions during the intervals between convective He-shell burning episodes (Straniero et al. 1995). The ^{13}C reaction, which operates at low temperatures ($kT \sim 8$ keV) and neutron densities ($n_n \leq 10^7$ cm^{-3}), provides most of the neutron exposure. The rate of the ^{13}C reaction has been adopted from Denker et al. (1995). However, the resulting abundances are modified by a second burst of neutrons from the ^{22}Ne(α, n)^{25}Mg reaction, which is marginally activated during the next convective instability, when higher temperatures ($kT \sim 23$ keV) are reached in the bottom layers of the convective pulse, leading to peak neutron densities of $n_n \leq 10^{10}$ cm^{-3} (Gallino et al. 1998). The rate of the ^{22}Ne reaction, which determines the strength of this neutron source, has been adopted from the evaluation of Käppeler et al. (1994), excluding the contribution by the resonance at 633 keV and using the lower limit for the width of the resonance at 828 keV. Fig. 3 shows a schematic representation of the sequence of He-shell flashes and the alternating interpulse periods.

The ^{13}C is produced via the reaction sequence ^{12}C(p, γ)^{13}N(β^+)^{13}C, when a small amount of protons is diffusing from the envelope into the top layers of the He- and ^{12}C-rich zone, forming the so-called ^{13}C pocket. This proton diffusion is supposedly driven by the occurrence of the third dredge-up episode, when H burning is temporarily inactive and the convective envelope penetrates into the upper region of the He intershell.

Although the second burst accounts only for a few percent of the total neutron exposure, it determines the final abundance patterns of the *s*-process branchings. This makes the

branchings a sensitive test for the interplay of the two neutron sources as well as for the time dependence of neutron density and temperature during the second neutron burst. In this context, it is important to note that the (n,γ) cross sections in the Te-I-Xe region are large enough that the typical neutron capture times are significantly shorter than the duration of the neutron exposure during the He shell flash.

As far as the isotopic abundance pattern of xenon is concerned, the current set of AGB models, covering a range of stellar masses ($1.5 \leq M/M_{\odot} \leq 3$) and metallicities ($-0.5 \leq$ [Fe/H] ≤ 0), was found to yield surprisingly consistent results. Changing the amount of ^{13}C, and hence the integrated neutron flux as well as the (α,n) rates of ^{13}C and ^{22}Ne by a factor of two, affected the ^{128}Xe/^{130}Xe ratios by less than 1.5%. This is remarkable, since the ^{13}C pocket determines the actual efficiency for neutron capture nucleosynthesis, whereas the ^{22}Ne rate governs the neutron density during He flashes. The effects due to variations of the most sensitive nuclear and stellar quantities are summarized in Tables 3 and 4.

In view of the robustness of the ^{128}Xe/^{130}Xe ratios with respect to the parameterization of the models used, the current calculations of AGB nucleosynthesis were based on the standard assumptions, which have been shown to match the solar main s-process component (Arlandini et al. 1999), i.e. using the average of models for 1.5 $M_{\odot}$ and 3 $M_{\odot}$, a metallicity of 0.5 $Z_{\odot}$, and the standard ^{13}C pocket (Busso et al. 1999; Gallino et al. 1998). Keeping the standard parameters unchanged, the resulting xenon abundances allowed us to study the effect of the time scales.

4.2. Convection in He shell flashes

Preliminary studies of the convective zone, generated by He shell flashes, reported turnover times of a few hours (Hollowell & Iben 1988). In this work, extensive calculations were carried out in order to study the possible effect on the branchings at ^{127}Te and ^{128}I more detailed.

The evolution of the internal structure of AGB stars was calculated for an initial mass range between 1 and 3 $M_{\odot}$. Convective velocities are evaluated by means of the mixing length theory. The numerical algorithms and the input physics of the *FRANEC* code used in this work have been extensively presented elsewhere (Straniero et al. 1997; Chieffi et al. 1998).

The results for a typical thermal pulse of a 3 $M_{\odot}$ AGB star of solar composition are summarized in Fig. 4. The temperature in the convective shell (top) is shown as a function of the mass coordinate for two different times (27 days before and 23 days after the maximum of the thermal pulse, respectively). The corresponding calculated convective velocities are

plotted in the panels below, showing the dependence on the mass coordinate (middle) and on the internal radius (bottom). The scale on the abscissa starts at the bottom of the convective shell. A comparison of the latter plots shows how the convective shell expands after the pulse maximum, while remaining almost constant in mass. The convective turnover time is only ≈1 hour.

This picture changes with core mass: the larger the core mass the higher are both, the peak of the bottom temperature and the peak of the convective velocity. The core mass of about 0.62 $M_{\odot}$ of the model shown in Fig. 4 is typical for a low mass AGB star. In fact, during the AGB phase the core mass increases from about 0.56 to 0.66 for initial stellar masses ranging from 1.5 to 3 $M_{\odot}$. Thus, temperatures as well as convective velocities of the intershell are increasing during the evolution along the AGB. With increasing stellar masses, the core mass at the beginning of the AGB phase becomes larger, resulting in a corresponding increase of temperatures and convective velocities.

Convective velocities are averages, which depend on the degree of super-adiabacity and on the adopted mixing length. Since convection is very efficient in stellar interiors, the degree of super-adiabacity is very small, leaving the mixing length as the main source of uncertainty. As usual, the mixing length parameter was calibrated by fitting the solar radius. The mixing length may realistically range between one and two pressure scale heights. Accordingly, the convective velocities may vary within a factor of two, because they depend linearly on the mixing length.

The short convective turnover time ensures that ^{128}I is efficiently removed from the hot reaction zone in spite of its 25 min half-life. From Fig. 4 one can infer that freshly produced material leaves the bottom zone within only 50 to 200 s. Accordingly, ^{128}I decays predominantly at lower temperatures, thus favoring the EC branch towards ^{128}Te, which yields correspondingly smaller ^{128}Xe/^{130}Xe ratios.

5. Results and discussion

The *s*-process nucleosynthesis calculation has been performed using a post-processing technique that carefully follows the stellar evolutionary structure up to the tip of the AGB (for details, see Section 2 of Gallino et al. 1998).

5.1. *s*-Process analyses

The results of the branching analyses are summarized in Table 5, which lists the calculated isotopic ratios for the *s*-only nuclei ^{128}Xe and ^{130}Xe. The respective uncertainties are essentially determined by the 1.5% uncertainty of the cross section ratio $\sigma(^{128}\mathrm{Xe})/\sigma(^{130}\mathrm{Xe})$ itself (Reifarth et al. 2002) as well as by the small uncertainties of the stellar branching ratio of ^{128}I discussed below.

While the first line of Table 5 illustrates the argument that the high temperature imposed by the classical model is not compatible with the ^{128}Xe/^{130}Xe ratios in Xe-S, the last lines refer to the stellar model results, which show a more promising behavior.

Since the decay of ^{128}I is dominated by the β^--mode, the results are insensitive to the stellar EC rate: Variations by a factor of two affect the branching ratio by less than 3%. This shows the robustness of the stellar model against changes in the stellar environment, resulting in an overall uncertainty of less than 3%.

A first hint that convection in the He shell has a noticeable effect on the branching was observed by comparing the ^{128}Xe/^{130}Xe ratios obtained with the *NETZ* code (Jaag 1991), which follows the *s*-process network with the neutron density and temperature profiles from the full AGB model, but neglects the effect of convection. These results yield ^{128}Xe/^{130}Xe ratios that are systematically higher than calculated with the full AGB model.

In the full model, the effect of convection on the abundance evolution was studied by reducing the time steps from the usually adopted 10^6 s to 10^5 s and eventually to 3×10^4 s (or 8 h). Though this led to a small effect on the ^{128}Te production via the branching at ^{127}Te, the net effect on the final ^{128}Xe/^{130}Xe ratio is negligible due to the rearrangement of the abundance pattern during freeze-out, when the neutron density is decreasing at the end of the pulse.

The change in the production factors during typical shell flashes

$$\frac{^{i}\mathrm{Xe}(t)/^{i}\mathrm{Xe}_{\odot}}{^{130}\mathrm{Xe}_{end}/^{130}\mathrm{Xe}_{\odot}}$$

are shown in Fig. 5 together with the time dependence of the average neutron density in the convective zone. The production factors are plotted relative to the ^{130}Xe abundance at the end of the shell flash and are normalized to the solar values. Obviously, the increase of temperature at the bottom of the convective shell with stellar mass and with pulse number is reflected by an increasing peak neutron density released by the $^{22}\mathrm{Ne}(\alpha,n)^{25}\mathrm{Mg}$ reaction.

The variations found in Fig. 5 confirm the more complex situation sketched in §4.2 than one might expect from the trends of the branching factor given in Table 2. During the low

temperature phase between He shell flashes, the neutron density produced via the ^{13}C(α, n)^{16}O reaction is less than 10^7 cm^{-3}. The neutron capture branch at ^{127}Te being completely closed results in a ^{128}Xe/^{130}Xe abundance ratio of 0.94 relative to the solar values at the end of the low temperature phase due to the effect of the ^{128}I branching. After the onset of convection and mixing with material from previous flashes at the beginning of the He shell flash, one finds the 8% difference between ^{128}Xe and ^{130}Xe, which is then modified as shown in Fig. 5.

During the following shell flash, the branching remains open in spite of the higher temperatures of this phase. There are three essential effects, which concur to explain this behavior:

- During the peak of temperature and neutron density, the electron densities at the bottom of the convective He shell flash, i.e. in the *s*-process zone, are between 15 $\times$ 10^{26} cm^{-3} and 20 $\times$ 10^{26} cm^{-3}. According to Table 2, the branching at ^{128}I is never completely closed. Even at the peak temperatures of the He-shell flash, typically 3% of the flow are bypassing ^{128}Xe.

- The quick transport of ^{128}I from the production zone to cooler layers implies that the EC decay branch remains significant. This causes more of the reaction flow to bypass ^{128}Xe and leads to smaller ^{128}Xe/^{130}Xe ratios.

- Around the maximum of the neutron density, the branching at ^{127}Te is no longer negligible. Instead, it leads to a significant effect on the ^{128}Xe abundance, which is more pronounced for the 25th pulse of the 3 $M_\odot$ model shown in the top panel of Fig. 5. Correspondingly, this branching is responsible for an *s*-process contribution of about 3% to the abundance of ^{128}Te, which is considered as an *r*-only isotope.

After averaging over the AGB evolution of the two stellar models for 1.5 and 3 $M_\odot$ with a metallicity of $0.5Z_\odot$, as described by Arlandini et al. (1999), we find an abundance ratio of (^{128}Xe/^{130}Xe)$_s$ = 0.466$\pm$0.015. This ratio corresponds to the He shell material, which is cumulatively mixed with the envelope by the recurrent third dredge-up episodes and eventually dispersed in the interstellar medium by efficient stellar winds. Consequently, it allows the solar ^{128}Xe abundance to contain a 9% *p*-process contribution. As an estimate for the Galactic average at the formation of the solar system, a ratio of (^{128}Xe/^{130}Xe)$_s$ = 0.468 was obtained by renormalizing the result of Travaglio et al. (1999) on the basis of the new Xe(n,γ) cross sections. This value represents the *s*-process evolution in the Galaxy by integrating over all previous generations of AGB stars of different masses and different metallicities. The observed ratio of 0.447$\pm$0.003 in the Xe-S component can only

be approached, if the remaining uncertainties are considered, in particular in the nuclear physics data and in the choice of the ^{13}C pocket (Table 4).

In summary, the combined effects of mass density, temperature, neutron density, and convective turnover appear to be consistently described, resulting in the successful reproduction of the solar ^{128}Xe/^{130}Xe ratio. This result represents an additional test of the employed stellar *s*-process models related to thermally pulsing low mass AGB stars.

Apart from the models discussed, other *s*-process scenarios do not contribute to the Xe-S problem. In particular, the weak *s*-process component related to helium burning in massive stars of 10 to 25 $M_\odot$ can be neglected. This was confirmed by calculations using the *NETZ* code with the temperature and neutron density profiles from a model for a 25 $M_\odot$ star (Raiteri et al. 1993). Normalization of the resulting abundance distribution to the *s*-only nuclei ^{70}Ge and ^{76}Se showed that less than 0.4% of the solar xenon abundance could be accounted for in this scenario.

5.2. Other processes

While the stellar models confirm the isotopic pattern of Xe-S to be, indeed, of *s*-process origin, the excess of ^{128}Xe in solar material has to be ascribed to a different source, most likely to the *p* process.

In spite of considerable uncertainties, network calculations for *p*-process nucleosynthesis in explosively burning Ne/O layers of type II supernovae (Rayet et al. 1995) indicate a significant contribution to the ^{128}Xe abundance, whereas the *p* production of ^{130}Xe is much less efficient. By normalizing the yields to the *p*-only nuclei ^{124,126}Xe, different SN II models find *p* contributions to the solar ^{128}Xe abundance of 25% (Rayet et al. 1995; M. Rayet, private communication) and 12% (Prantzos et al. 1990), respectively. A study of the *p* process in type Ia supernovae (Howard et al. 1991) yielded a *p*-abundance ratio ^{124}Xe/^{126}Xe that differs by a factor of three from the solar value, corresponding to an 8% *p* contribution to the solar ^{128}Xe abundance. Recently, full nucleosynthesis calculations following the hydrostatic and explosive phases of massive stars by Rauscher et al. (2002) have provided similar results for an enhanced *p*-process yield of ^{128}Xe compared to ^{130}Xe.

Contributions from alternative nucleosynthesis mechanisms, like the *rp* and the ν-processes, can be excluded. The *rp* process can be ruled out, because reaction path ends at $A \approx 107$ in the Sn-Sb-Te cycle (Schatz et al. 2001). Detailed calculations showed that the ν process contribution to the xenon abundance distribution is negligible (Woosley et al. 1990).

6. Summary

The solar abundances of ^{128}Xe and ^{130}Xe are produced by the main component of the s process, except for a non-negligible p contribution to ^{128}Xe. By comparison with pure s-process xenon, i.e. the Xe-S found in presolar grains, this p component amounts to 9±3%, thus providing an additional constraint for p-process calculations.

The s-process reaction flow through the branchings at ^{127}Te and ^{128}I has been followed in detail with stellar evolutionary models for the asymptotic giant branch (AGB) phase. It was found that the solar abundances as well as the Xe-S ratio of ^{128}Xe and ^{130}Xe could be successfully reproduced. Since these branchings exhibit a much weaker dependence on neutron density than other cases, they represent an important complement to all previous branching analyses (Arlandini et al. 1999; Best et al. 2001). Apart from an small additional effect of the electron or mass density it turned out that the short half-life of the ^{128}I branch point represents a first constraint for the convective velocities during the He shell flash. In view of the complex interplay of all these parameters, the consistent description of the ^{128}Xe/^{130}Xe ratio can be considered as a further successful test of the AGB models used.

The lower ^{128}Xe/^{130}Xe ratio measured in presolar mainstream SiC grains compared to the solar abundance ratio corresponds to the situation in thermal pulses during the last part of the AGB phase, which exhibit higher temperatures and neutron densities. This confirms that the mainstream SIC grains, the carriers of the Xe-S meteoritic component, were predominantly formed during this epoch.

The impact of the fast convective turnover time scale found in the present study is also of potential interest for other, previously neglected branchings.

We would like to thank U. Ott, R. Pepin, and M. Rayet for clarifying discussions. R.R. is indebted to CERN for support by the doctoral student program. This work was partly supported by the Italian MIUR-FIRB grant "The astrophysical origin of the heavy elements beyond Fe".

REFERENCES

Anders, E., & Grevesse, N. 1989, Geochim. Cosmochim. Acta, 53, 197

Arlandini, C., Käppeler, F., Wisshak, K., Gallino, R., Lugaro, M., Busso, M., & Straniero, O. 1999, ApJ, 525, 886

Best, J., Stoll, H., Arlandini, C., Jaag, S., Käppeler, F., Wisshak, K., Mengoni, A., Reffo, G., & Rauscher, T. 2001, Phys. Rev. C, 64, 15801

Busso, M., Gallino, R., & Wasserburg, G.J. 1999, ARA&A, 37, 239

Chieffi, A., Limongi, M., & Straniero, O. 1998, ApJ, 502, 737

De Laeter, J., & Barnest, I.L. 1991, Pure Appl. Chem., 63, 991

Denker, A., Drotleff, H.W., Grosse, M., Knee, H., Mayer, A., Seidel, Soiné, R., Wöhr, A., Wolf, G., & Hammer, W. 1995 in *Nuclei in the Cosmos III*, edited by M. Busso, C.M. Raiteri, & R. Gallino, AIP Conf. Proc. 327 (AIP, New York, 1995) 255

Gallino, R., Arlandini, C., Busso, M., Lugaro, M., Travaglio, C., Straniero, O., Chieffi, A., & Limongi, M. 1998, ApJ, 497, 388

Goriely, S. 1999, A&A, 342, 881

Hollowell, D., & Iben, I. Jr. 1988, ApJ, 333, L25

Howard, W.M., Meyer, B.S., & Woosley, S.E. 1991, ApJ, 373, L5

Huss, G.R. & Lewis, R.S. 1994, Meteoritics, 29, 791

Iben, I. Jr., & Renzini, A. 1983, ARA&A, 21, 271

Jaag, S. NETZ - Internal report 14.01.01/p35g. Forschungszentrum Karlsruhe, 1991

Käppeler, F., Wiescher, M., Giesen, U., Görres, J., Baraffe, I., El Eid, M., Rateri, C.M., Busso, M., Gallino, R., Limongi, M., & Chieffi, A. 1994, ApJ, 437, 396

Lewis, R.S., Amari, S., & Anders, E. 1994, Geochim. Cosmochim. Acta, 58, 471

Ott, U. 1993, Nature, 364, 25

Pepin, R.O., Becker, R.H., & Rider, P.E. 1995, Geochim. Cosmochim. Acta, 59, 4997

Prantzos, N., Hashimoto, M., Rayet, M., & Arnould, M. 1990, A&A, 238, 455

Raiteri, C.M., Gallino, R., Busso, M., Neuberger, D., & Käppeler, F. 1993, ApJ, 419, 207

Rapp, D., Naderi, F., Neugebauer, M., Sevilla, D., Sweetnam, D., Wiens, R., Burnett, D., Smith, N., Clark, B., McComas, D., & Stansbery, E. 1996, Acta Astron., 39, 229

Rayet, M., Arnould, M., Hashimoto, M., Prantzos, N., & Nomoto, K. 1995, A&A, 298, 517

Rauscher, T., Heger, A., Hoffman, R., & Woosley, S.E. 2002, ApJ, 576, 323

Reifarth, R., Heil, M., Käppeler, F., Voss, F., Wisshak, K., Bečvář, F., Krtička, M., Gallino, R., & Nagai, Y. 2002, Phys. Rev. C, 66, 064603

Reifarth, R., & Käppeler, F. 2002, Phys. Rev. C, 66, 054605

Reynolds, J.H., & Turner, G. 1964, J. Geophys. Res., 69, 3263

Schatz, H., Aprahamian, A., V., Barnard, Bildsten, L., Cumming, A., Ouellette, M., Rauscher, T., Thielemann, F.-K., & Wiescher, M. 2001, Phys. Rev. Letters, 86, 3471

Straniero, O., Gallino, R., Busso, M., Chieffi, A., Raiteri, C.M., Limongi, M., & Salaris, M. 1995, ApJ, 440, L85

Straniero, O., Chieffi, A., & Limongi, M. 1997, ApJ, 490, 425

Takahashi, K., & Yokoi, K. 1987, Atomic Data Nucl. Data Tables, 36, 375

Travaglio, C., Galli, D., Gallino, R., Busso, M., Ferrini, F., & Straniero, O. 1999, ApJ, 521, 691

Woosley, S.E., & Howard, W.M. 1978, ApJS, 36, 285

Woosley, S.E., Hartmann, D.H., Hoffman, R.D., & Haxton, W.C. 1990, ApJ, 356, 272

Zinner, E. 1998, Annu. Rev. Earth Planet. Sci., 26, 147

This preprint was prepared with the AAS LaTeX macros v5.2.

Table 1. Different abundance ratios of ^{128}Xe and ^{130}Xe

Abundance ratio ^{128}Xe/^{130}Xe	Reference	Remark
0.466 ± 0.014	(De Laeter & Barnest 1991)	terrestrial
0.503	(Anders & Grevesse 1989)	solar
0.510 ± 0.005	(Pepin et al. 1995)	solar
0.447 ± 0.003	(Lewis et al. 1994)	Xe-S (SiC)
0.586 ± 0.004	(Huss & Lewis 1994)	Xe-HL (Diamond)

Table 2. Beta-decay branching ratio at ^{128}I as a function of electron density and temperature (Takahashi & Yokoi 1987).

Electron density (10^{26} cm^{-3})	Temperature (10^8 K)					
	0	1	2	3	4	5
0	0.940	0.963	0.996	0.999	1.000	1.000
3	0.940	0.952	0.991	0.997	0.999	0.999
10	0.940	0.944	0.976	0.992	0.996	0.997
30	0.940	0.938	0.956	0.980	0.989	0.995

Table 3. The *s*-process ^{128}Xe/^{130}Xe ratios obtained by variation of the most sensitive nuclear quantities

^{128}I EC-rate[a]		^{13}C(α,n)^{16}O rate[b]		^{22}Ne(α,n)^{25}Mg rate[c]	
[Fe/H] = − 0.30	$(^{128}Xe/^{130}Xe)_s$	[Fe/H] = − 0.30	$(^{128}Xe/^{130}Xe)_s$	[Fe/H] = − 0.30	$(^{128}Xe/^{130}Xe)_s$
SR	0.466	SR	0.466	SR	0.466
SR/2	0.482	SR*2	0.471	SR*2	0.470
–	–	SR/2	0.468	SR/2	0.466

[a] standard rate (SR) from Takahashi & Yokoi (1987)
[b] standard rate (SR) adopted from Denker et al. (1994)
[c] standard rate (SR) adopted from Käppeler et al. (1994) as described in text

Table 4. The *s*-process ^{128}Xe/^{130}Xe ratios obtained by variation of the most sensitive stellar quantities

^{13}C-pocket[a]		Metallicity	
[Fe/H] = − 0.30	$(^{128}Xe/^{130}Xe)_s$	[Fe/H]	$(^{128}Xe/^{130}Xe)_s$
ST*2	0.446	0.0	0.460
ST	0.466	− 0.30	0.466
ST/2	0.465	− 0.52	0.461

[a] standard case (ST) chosen to match overall solar *s* abundances (Gallino et al. 1998)

Table 5. Results of the *s*-process calculations

Model	Abundance ratio ^{128}Xe/^{130}Xe	Remarks
classical model	0.51 ± 0.02	$kT = 29$ keV, ^{127}Te thermalized, *NETZ* code[a]
simplified AGB	0.477 ± 0.02	turnover neglected, *NETZ* code[a]
AGB[b], full network	0.473 ± 0.015	time steps of 10^6 s
AGB[b], full network	0.466 ± 0.015	time steps of 10^5 s

[a] (Jaag 1991)
[b](Gallino et al. 1998)

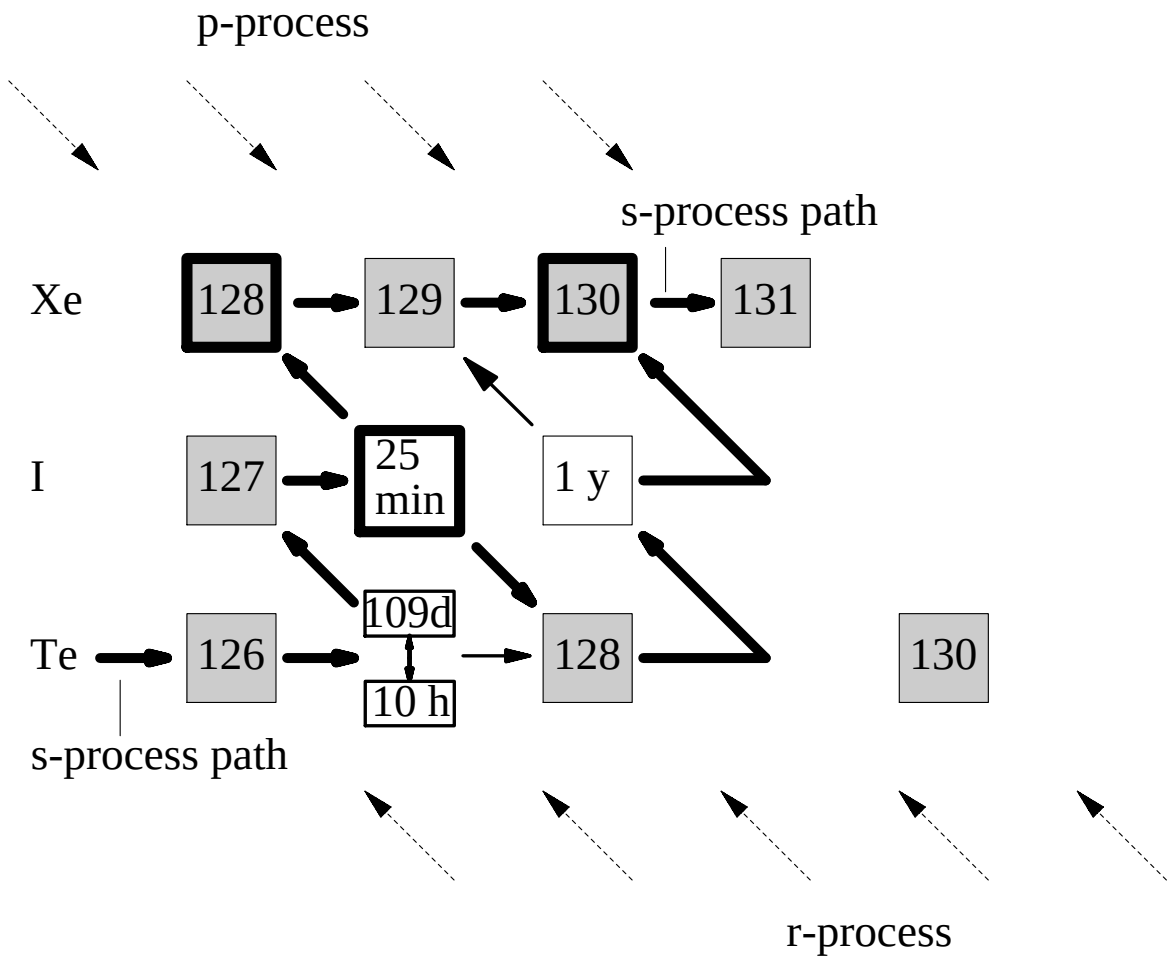

Fig. 1.— The s-process reaction path between Te and Xe. The isotopes ^{128}Xe and ^{130}Xe are shielded against r-process contributions by their stable Te isobars. In contrast to ^{130}Xe, ^{128}Xe is partly bypassed due to the branching at ^{128}I. The branching at ^{127}Te is negligible unless the temperature is low enough that ground state and isomer are not fully thermalized. The branching at ^{128}I is unique since it results from the competition between β^- and electron capture decays, independent of the neutron flux.

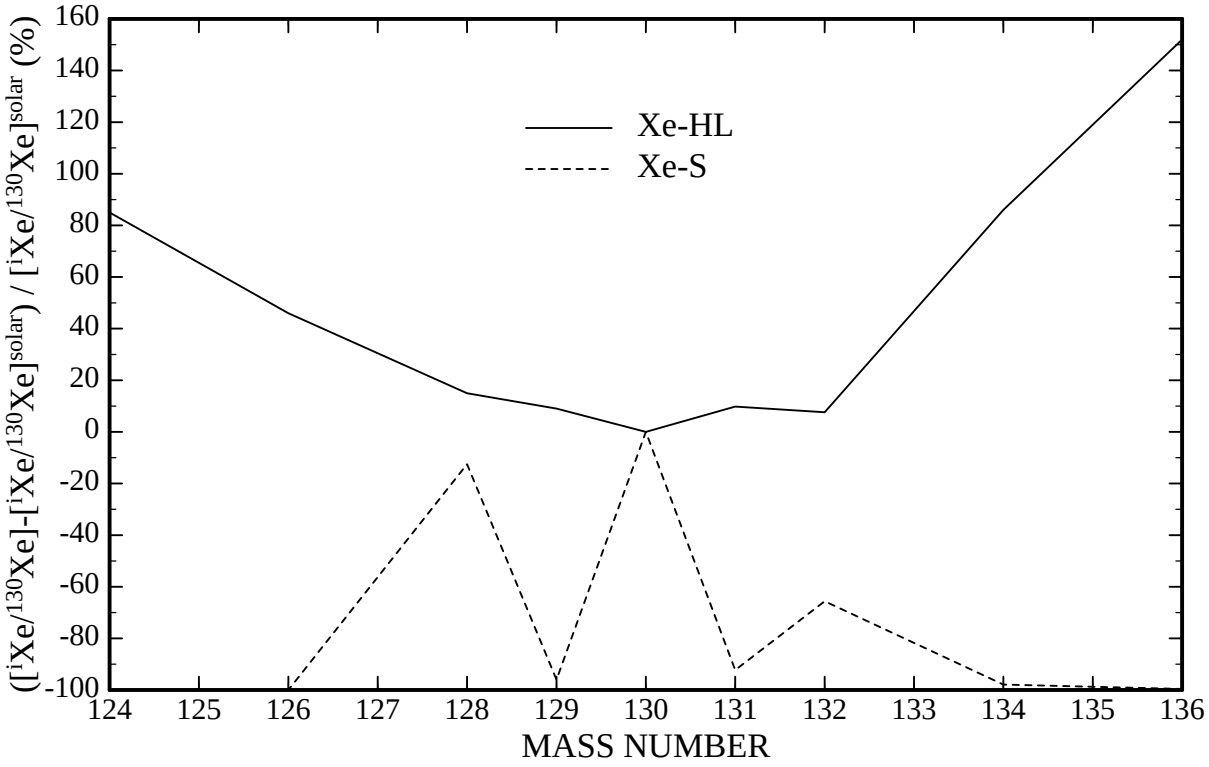

Fig. 2.— The abundance pattern of Xe-S (Lewis et al. 1994) relative to the solar distribution shows that the ratio of the *s* process isotopes 128 and 130 is 12% less than unity, indicating the effect of the ^{128}I branching. The *s* contributions to the other Xe isotopes are much smaller. Xe-HL, the counterpart from explosive nucleosynthesis is enhanced in the light and heavy isotopes produced in the *p* and *r* process, respectively (Huss & Lewis 1994). Fission may additionally contribute to $^{129,131-136}$Xe. The abundance patterns are normalized at ^{130}Xe.

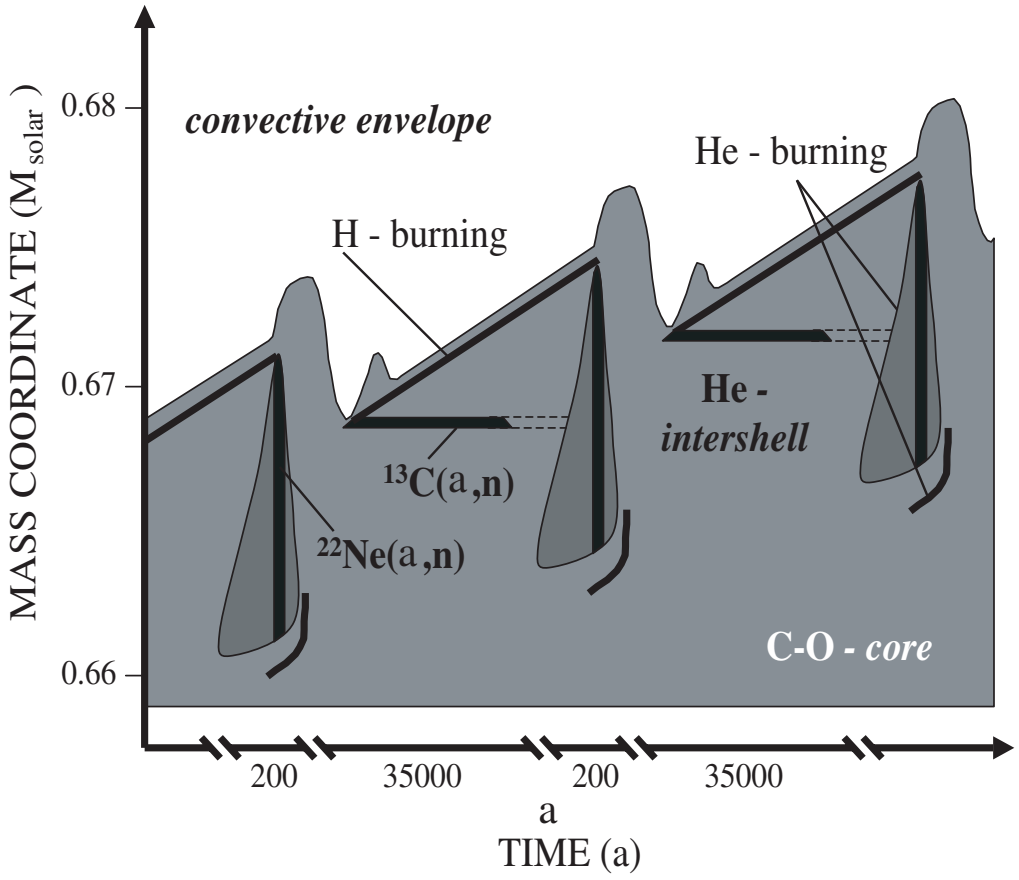

Fig. 3.— Schematic illustration of the *s*-process during the AGB-phase. The breaks in the time axis illustrate the shortness of the He shell flashes, lasting only a few hundred years, compared with the interpulse phase of about 35,000 yr. The mass coordinate (in $M_{\odot}$) indicates the thin He intershell, which is the site of the *s* process. The ^{13}C(α, n)^{16}O reaction represents the dominant neutron source, which operates during interpulse period, whereas the higher temperatures during the convective He shell flash eventually activate the ^{22}Ne(α, n)^{25}Mg reaction, which is important for establishing the abundance patterns of the *s*-process branchings (Gallino et al. 1998).

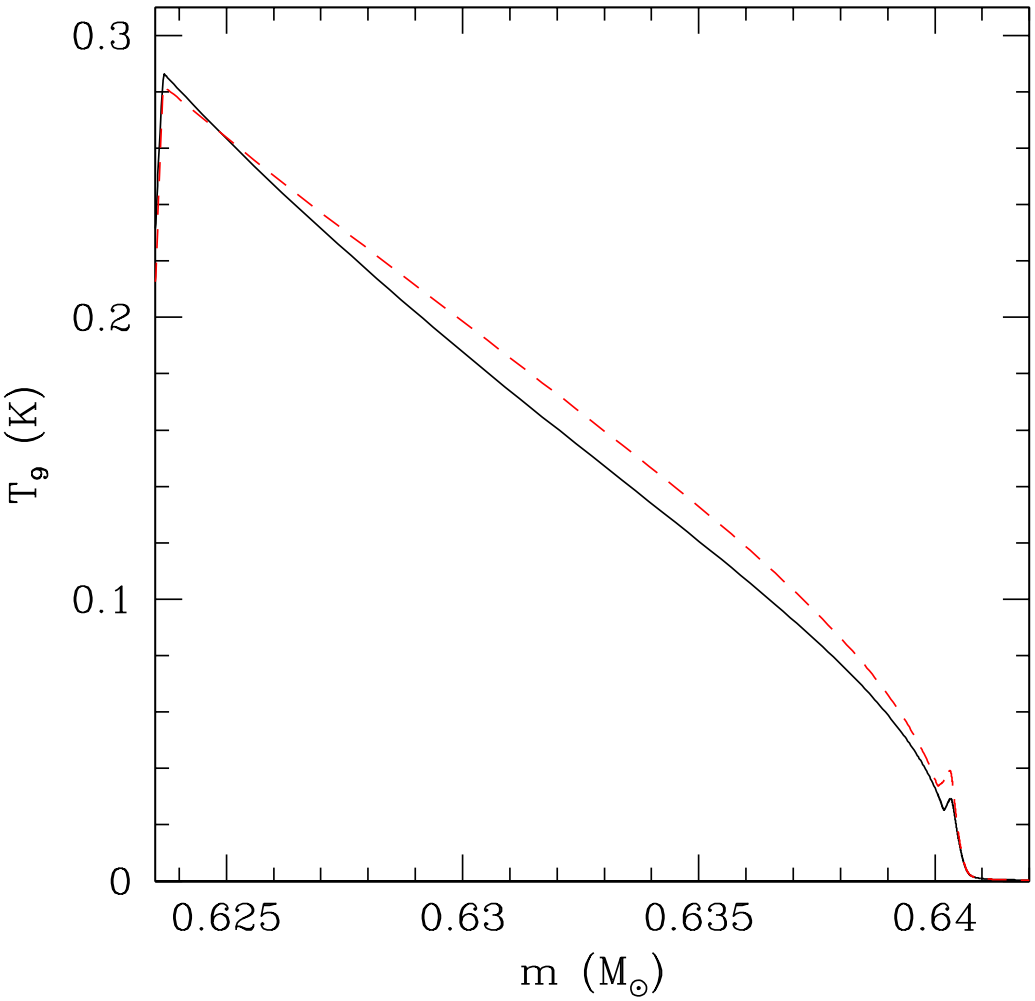
0.3
0.2
0.1
0
T_9 (K)
0.625
0.63
0.635
0.64
m ($M_\odot$)

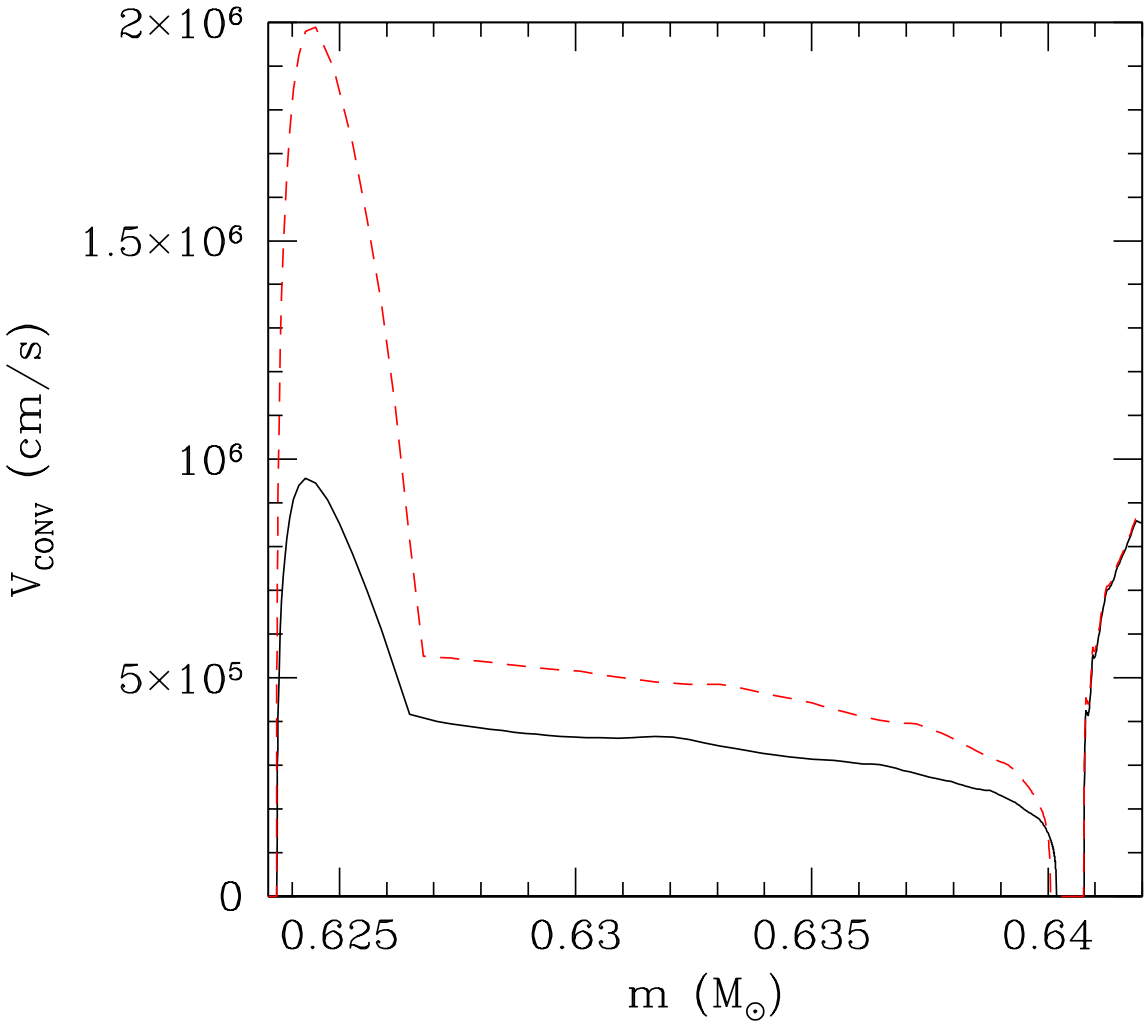
2×10⁶
1.5×10⁶
10⁶
5×10⁵
0
V_CONV (cm/s)
0.625
0.63
0.635
0.64
m (M⊙)

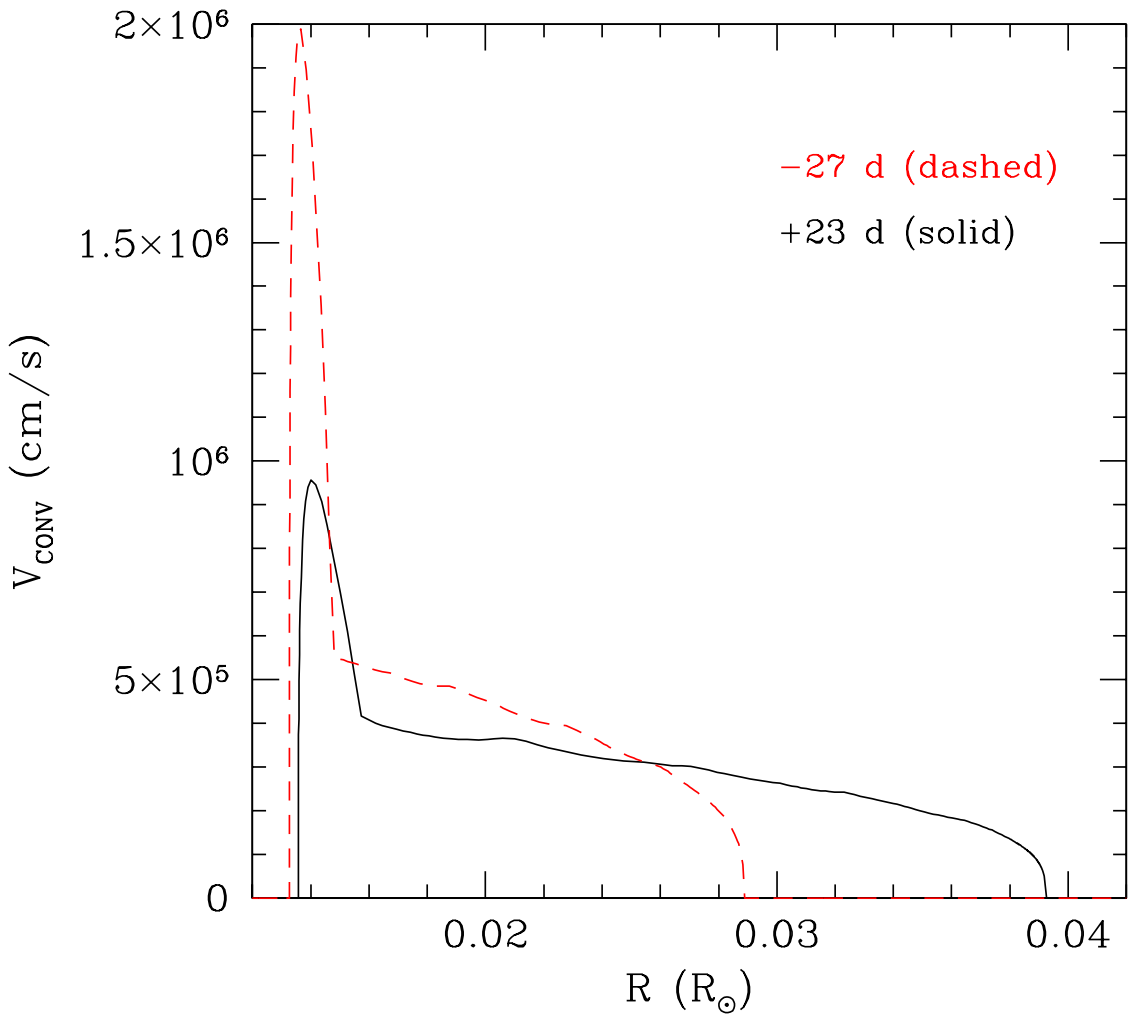

Fig. 4.— The temperature in the convective shell in a 3 $M_\odot$ star of solar composition during a typical thermal pulse (top) as a function of the mass coordinate for two different times, 27 d before and 23 d after pulse maximum (dashed and solid lines, respectively). The abscissa starts at the bottom of the convective shell. The corresponding convective velocities as a function of the mass coordinate (middle) and of the internal radius (bottom) are plotted below. The convective turnover time is ≈1 hour, but it takes only 50 to 200 s to transport freshly produced ^{128}I from the *s*-process zone in the bottom layers into the outer, cooler regions.

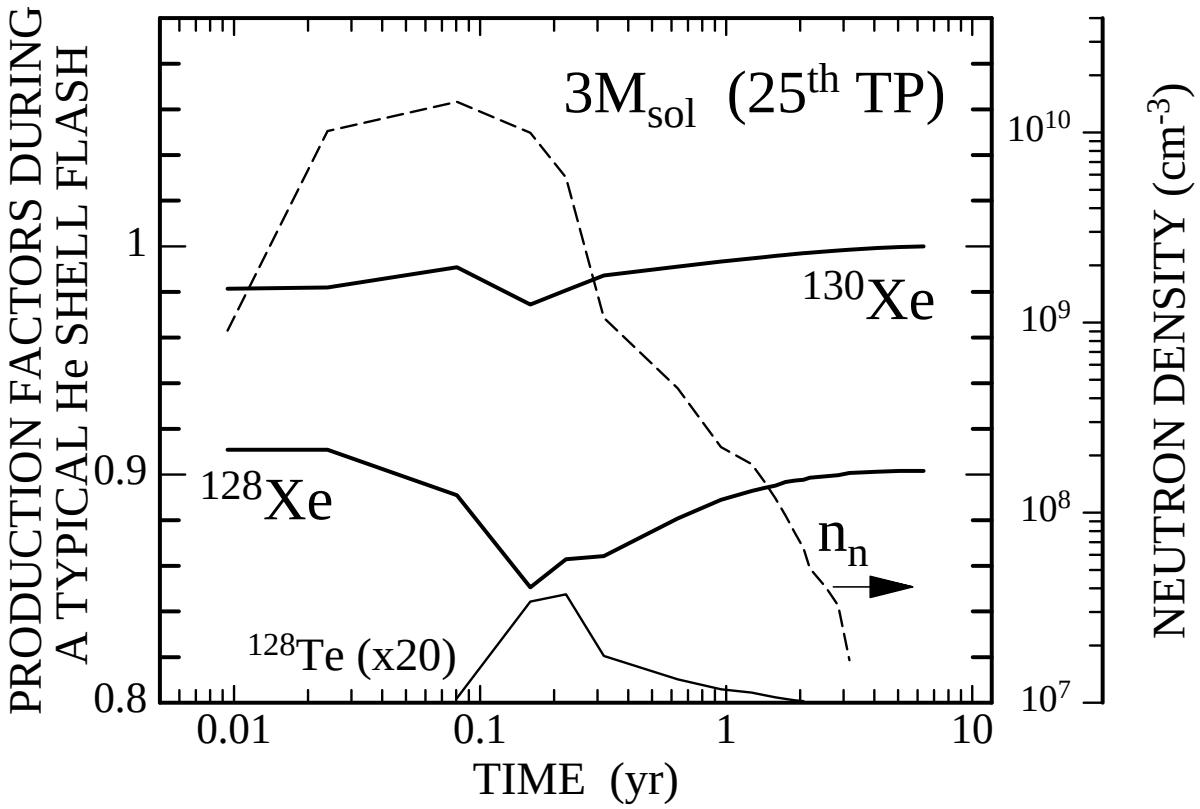
3M$_{sol}$ (25th TP)
^{130}Xe
^{128}Xe
^{128}Te (x20)
n$_n$
PRODUCTION FACTORS DURING A TYPICAL He SHELL FLASH
NEUTRON DENSITY (cm^{-3})
TIME (yr)
1
0.9
0.8
0.01
0.1
1
10
10^{10}
10^{9}
10^{8}
10^{7}

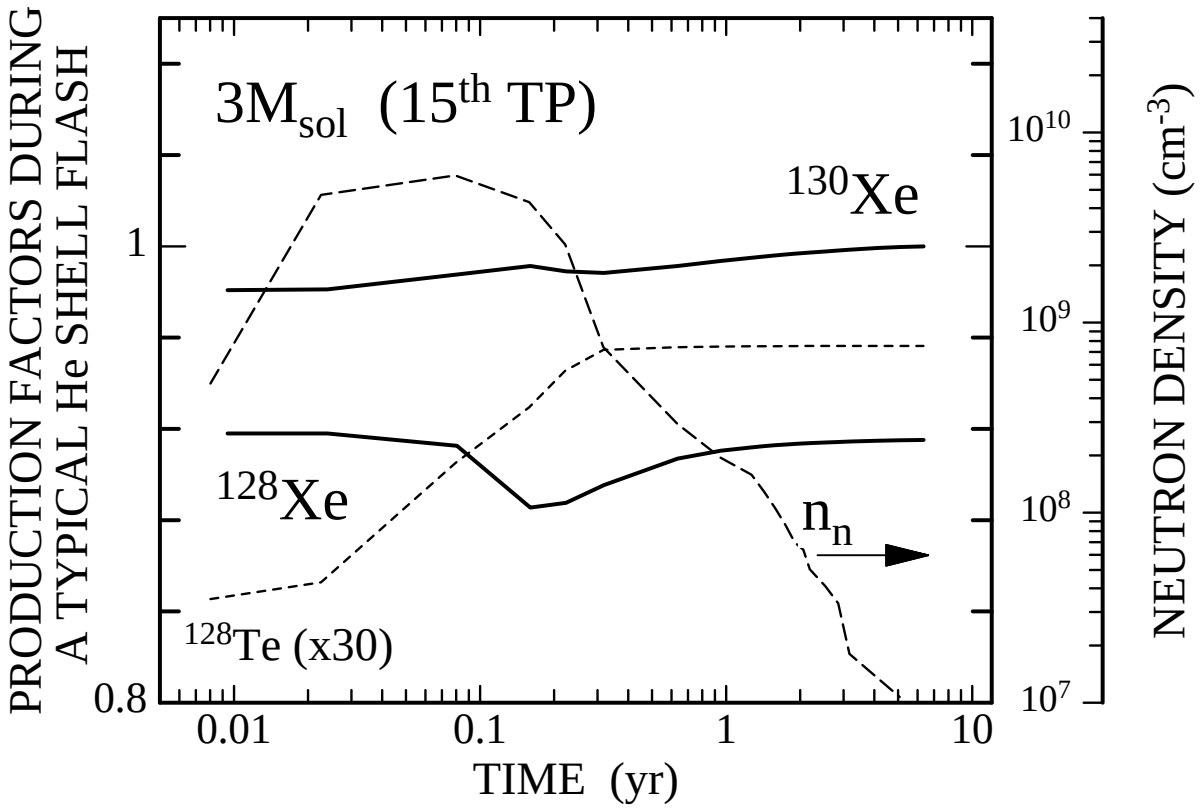
PRODUCTION FACTORS DURING
A TYPICAL He SHELL FLASH
3M$_{sol}$ (15th TP)
^{130}Xe
^{128}Xe
^{128}Te (x30)
n$_n$
1
0.8
0.01
0.1
1
10
TIME (yr)
10^{10}
10^{9}
10^{8}
10^{7}
NEUTRON DENSITY (cm^{-3})

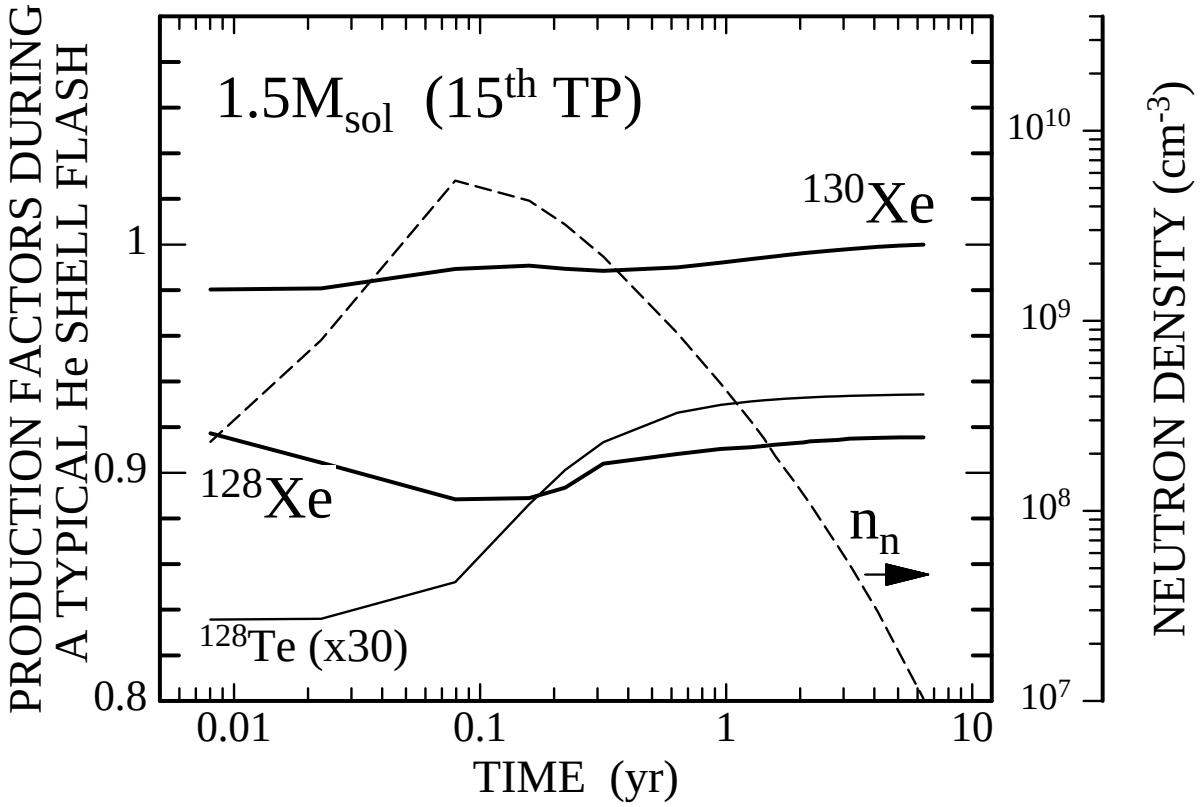

Fig. 5.— The production factors of ^{128}Xe and ^{130}Xe during typical He shell flashes in two AGB stars (top and middle: 25th and 15th pulse in a 3 $M_\odot$ star, bottom: 15th pulse in a 1.5 $M_\odot$ star). The time scale starts when the temperature at the bottom of the convective shell reaches 2.5×10^8 K, i.e. at the onset of the ^{22}Ne(α, n)^{25}Mg reaction. The curves are normalized to ^{130}Xe at the end of the shell flash as explained in the text. The average neutron density produced at the bottom of the convective region by the ^{22}Ne(α, n)^{25}Mg reaction is indicated by the dashed line. The production ratio of ^{128}Xe/^{130}Xe is always below unity, which implies that the branchings at A=127/128 remain active throughout the shell flash due to the combined effects of mass density, temperature, neutron density, and convective turnover times (see text).